Mixed Valency in $Yb_7Co_4InGe_{12}$: A Novel Intermetallic Compound Stabilized in Liquid Indium

Maria Chondroudi,[†,§] Mahalingam Balasubramanian,[‡] Ulrich Welp,[§] Wai-K. Kwok,[§] and Mercouri G. Kanatzidis*[,§,||]

Department of Chemistry, Michigan State University, East Lansing, Michigan 48824, Advanced Photon Source and Materials Science Division, Argonne National Laboratory, Argonne, Illinois 60439, and Department of Chemistry, Northwestern University, Evanston, Illinois 60208

Received June 24, 2007

The quaternary compounds $RE_7Co_4InGe_{12}$ (RE = Dy, Ho, Yb) were obtained from In flux reactions as thin silver needles. $RE_7Co_4InGe_{12}$ crystallizes in the tetragonal *P4/m* space group under a new structure type which is characterized by columnar units forming three different types of channels with the RE atoms situated within these channels. Investigation of the Yb analog with magnetic susceptibility measurements, X-ray photoelectron spectroscopy (XPS) and X-ray absorption near edge spectroscopy (XANES) revealed that $Yb_7Co_4InGe_{12}$ is a mixed-valence compound and that the relative Yb^{3+}/Yb^{2+} ratio is slightly temperature-dependent. Additionally, resistivity measurements for $Yb_7Co_4InGe_{12}$ exhibited negative magnetoresistance at low temperatures.

Introduction

Molten metals can be excellent solvents for the synthesis of new intermetallic compounds.[1] For example, molten Al when used to investigate the reactivity of the quaternary systems RE/TM/Si(Ge) (RE = rare earth metal, TM = transition metal) readily gave rise to new complex quaternary phases such as $Sm_2Ni(Si_{1-x}Ni_x)Al_4Si_6$,[2] $RE_8Ru_{12}Al_{49}Si_9$,[3] and $RE_2NiAl_4Ge_2$.[4] In these cases, a notable feature of this chemistry is the inclusion of Al into the crystal structure. Interestingly, when Ga was employed in analogous reactions within the RE/TM/Si system, it generally yielded Ga-free products (e.g., $SmNiSi_3$[5]) or Si-free products (e.g., $Sm_2Ni_3Si_5$[6] and Sm_2NiGa_{12}[7]). When Si is replaced by Ge in the Ga flux reactions, however, quaternary compounds such as $RE_3Ni_3Ga_8Ge_3$[8] and $GdCo_{1-x}Ga_3Ge$[8] are readily observed. These are surprising differences in reactivity given the close relationship of Al to Ga and Si to Ge, respectively. These results imply that there is much new chemistry and reactivity to be learned by studying fluxes of related elements.

Recently, we extended this work to include molten In as a solvent in the system RE/TM/Ge.[9,10] Indium has been extensively used for the crystal growth of primarily known binary and ternary phases;[1] however, it has been less exploited as a synthetic flux medium compared to Al and Ga, especially for quaternary compounds.[11−15] Our work in In flux has led to only a few quaternary phases such as the $RE_4Ni_2InGe_4$.[16]

Among intermetallics that are likely to be stabilized in metallic fluxes, the Yb-containing ones are particularly attractive because they can display intriguing properties caused by the diverse character of their f electrons.[17] These electrons can play a dynamic role in bonding, leading to intermediate valence, unusual magnetism, Kondo, and heavy fermion behavior, to name just a few.[18] Yb can exhibit two

* Corresponding author. E-mail: m-kanatzidis@northwestern.edu.
† Michigan State University.
§ Materials Science Division, Argonne National Laboratory.
‡ Advanced Photon Source, Argonne National Laboratory.
|| Northwestern University.

(1) Kanatzidis, M. G.; Pottgen, R.; Jeitschko, W. *Angew. Chem., Int. Ed.* **2005**, *44* (43), 6996−7023.
(2) Chen, X. Z.; Sportouch, S.; Sieve, B.; Brazis, P.; Kannewurf, C. R.; Cowen, J. A.; Patschke, R.; Kanatzidis, M. G. *Chem. Mater.* **1998**, *10* (10), 3202−3211.
(3) Sieve, B.; Chen, X. Z.; Henning, R.; Brazis, P.; Kannewurf, C. R.; Cowen, J. A.; Schultz, A. J.; Kanatzidis, M. G. *J. Am. Chem. Soc.* **2001**, *123* (29), 7040−7047.
(4) Sieve, B.; Trikalitis, P. N.; Kanatzidis, M. G. *Z. Anorg. Allg. Chem.* **2002**, *628* (7), 1568−1574.
(5) Chen, X. Z.; Larson, P.; Sportouch, S.; Brazis, P.; Mahanti, S. D.; Kannewurf, C. R.; Kanatzidis, M. G. *Chem. Mater.* **1999**, *11* (1), 75−83.
(6) Zhuravleva, M. A.; Kanatzidis, M. G. *Z. Naturforsch., Sect. B* **2003**, *58* (7), 649−657.
(7) Chen, X. Z.; Small, P.; Sportouch, S.; Zhuravleva, M.; Brazis, P.; Kannewurf, C. R.; Kanatzidis, M. G. *Chem. Mater.* **2000**, *12* (9), 2520−2522.
(8) (a) Zhuravleva, M. A.; Pcionek, R. J.; Wang, X. P.; Schultz, A. J.; Kanatzidis, M. G. *Inorg. Chem.* **2003**, *42* (20), 6412−6424. (b) Zhuravleva, M. A.; Evain, M.; Petricek, V.; Kanatzidis, M. G. *J. Am. Chem. Soc.* **2007**, *129*(11), 3082−3083.
(9) Salvador, J. R.; Bilc, D.; Gour, J. R.; Mahanti, S. D.; Kanatzidis, M. G. *Inorg. Chem.* **2005**, *44* (24), 8670−8679.
(10) Salvador, J. R.; Gour, J. R.; Bilc, D.; Mahanti, S. D.; Kanatzidis, M. G. *Inorg. Chem.* **2004**, *43* (4), 1403−1410.
(11) Bailey, M. S.; McGuire, M. A.; DiSalvo, F. J. *J. Solid State Chem.* **2005**, *178* (11), 3494−3499.
(12) Benbow, E. M.; Latturner, S. E. *J. Solid State Chem.* **2006**, *179* (12), 3989−3996.
(13) Klunter, W.; Jung, W. *J. Solid State Chem.* **2006**, *179* (9), 2880−2888.
(14) Lukachuk, M.; Galadzhun, Y. V.; Zaremba, R. I.; Dzevenko, M. V.; Kalychak, Y. M.; Zaremba, V. I.; Rodewald, U. C.; Pottgen, R. *J. Solid State Chem.* **2005**, *178* (9), 2724−2733.
(15) Zaremba, V. I.; Dubenskiy, V. P.; Rodewald, U. C.; Heying, B.; Pottgen, R. *J. Solid State Chem.* **2006**, *179* (3), 891−897.
(16) Salvador, J. R.; Kanatzidis, M. G. *Inorg. Chem.* **2006**, *45* (18), 7091−7099.
(17) Lawrence, J. M.; Riseborough, P. S.; Parks, R. D. *Rep. Prog. Phys.* **1981**, *44* (1), 1−84.
(18) Kindler, B.; Finsterbusch, D.; Graf, R.; Ritter, F. *Phys. Rev. B* **1994**, *50*(2), 704−707.

10.1021/cm071687q CCC: $37.00
Published on Web 08/21/2007

valence states concerning the nonmagnetic $4f^{14}$ (Yb^{2+}) and magnetic $4f^{13}$ (Yb^{3+}) electronic configurations. For this reason, we investigated the reactivity of the Yb/Co/Ge system in liquid indium. Here, we present $Yb_7Co_4InGe_{12}$ as well as the Dy and Ho analogs, which are ordered quaternary intermetallic compounds with a new structure type. This is only the second example after $RE_4Ni_2InGe_4$ in which In is acting as a reactive flux in the RE/TM/Ge system. The Yb analog is a mixed-valence compound with predominant Yb^{3+} ions and exhibits negative magnetoresistance.

Experimental Section

Reagents. The following reagents were used as purchased without further purification: Yb, Dy, Ho (in the form of powder ground from metal chunk, 99.9%, Chinese Rare Earth Information Center, Inner Mongolia, China), Co (−325 mesh 99.9%, Cerac Milwaukee WI), Ge (ground from 2−5 mm pieces, 99.999%, Plasmaterials Livermore, CA) and In (tear drops, 99.99%, Cerac Milwaukee, WI).

Synthesis. *Method A:* The $RE_7Co_4InGe_{12}$ (RE = Dy, Ho, Yb,) compounds were obtained by combining 3 mmol of the corresponding rare earth metal, 2 mmol of cobalt, 3 mmol of germanium, and 15 mmol of indium in an Al_2O_3 (alumina) crucible under an inert nitrogen atmosphere inside a glovebox. The crucible was placed in a 13 mm fused silica tube, which was flame sealed under a vacuum at 1×10^{-4} Torr to prevent oxidation during heating. The reactants were then heated to 1000 °C over the course of 10 h and maintained at that temperature for 4 h to allow proper homogenization, followed by being cooled to 850 °C in 2 h and held there for 48 h. Finally, the system was allowed to slowly cool to 50 °C in 48 h. The reaction product was isolated from the unreacted In by heating at 350 °C and subsequent centrifugation through a coarse frit. The remaining flux was removed by immersion and sonication in glacial acetic acid for 48 h. The final crystalline product was rinsed with water and dried with acetone. The yields of the reactions were 20−70%, with purity ranging from 30 to 80% depending on the RE metal. Several crystals, which grow as metallic silver needles and tend to aggregate, were carefully selected for elemental analysis, structure characterization, differential thermal analysis, magnetic susceptibility, XPS, XANES, and resistivity measurements.

Method B: $Yb_7Co_4InGe_{12}$ was also prepared by combining 6 mmol of ytterbium metal, 2 mmol of cobalt, 5 mmol of germanium, and 15 mmol of indium in an Al_2O_3 (alumina) crucible under an inert nitrogen atmosphere inside a glovebox. The reactants were then heated under the same heating profile as in method A. This method increased the purity (90%) and the yield (80%) of the target phase. Attempts to generate the $Yb_7Co_4InGe_{12}$ phase by direct combination of the elements in their stoichiometric ratios and heating in a RF induction heating furnace were not successful.

Elemental Analysis. Semiquantitative microprobe elemental analysis was performed on several crystals of the compound using a JEOL JSM-35C scanning electron microscope (SEM) equipped with a Noran Vantage energy-dispersive spectroscopy (EDS) detector. Data were acquired by applying a 25 kV accelerating voltage and an acquisition time of 40 s. A typical needlelike crystal of $Yb_7Co_4InGe_{12}$ is shown in Figure 1. The EDS analysis taken on visibly clean surfaces of the $Yb_7Co_4InGe_{12}$ crystals gave the atomic composition of 31.5% Yb, 17.3% Co, 3.9% In, and 48.4% Ge ($Yb_8Co_{4.4}InGe_{12.5}$), which is in good agreement with the results derived from the single-crystal X-ray diffraction refinement. Similar stoichiometric ratios were determined for the other RE analogs as well.

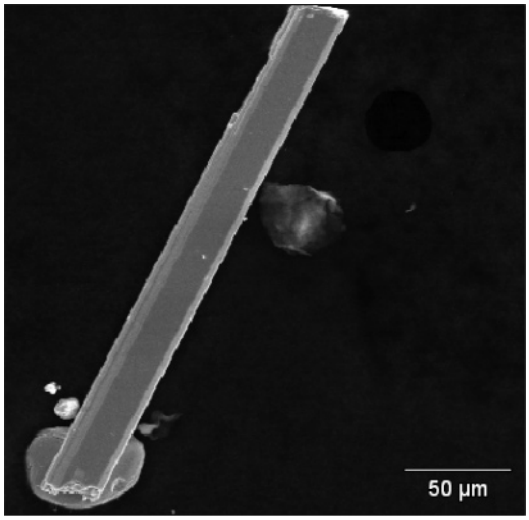

Figure 1. Scanning electron micrograph (SEM) image of a flux-grown $Yb_7Co_4InGe_{12}$ crystal.

X-ray Crystallography. The X-ray intensity data were collected at room temperature using a Bruker SMART Platform CCD diffractometer with graphite-monochromatized Mo Ka ($\lambda = 0.71073$ Å) radiation. The SMART software was used for data acquisition and SAINT for data extraction and reduction.[19] An empirical absorption correction was applied using the program SADABS[19] and the structure of $Yb_7Co_4InGe_{12}$ was solved by direct methods and refined with the SHELXTL package programs.[20] A stable refinement was accomplished only in the tetragonal space group *P*4/*m*. Standardization of the atomic positions of $Yb_7Co_4InGe_{12}$ was performed with Platon-Structure Tidy application of the WinGX package software.[21] Solutions of the Dy and Ho analogs were obtained by using the solution of $Yb_7Co_4InGe_{12}$ as a starting point, with the final refinement done using SHELXTL. Interestingly, the Co and Ge(2) positions in the Dy and Ho analogs are switched compared to the Yb analog, and the Ge(3) atom is repositioned. This model gave far better *R* values. For example, for the Dy and Ho analogs, we obtain $R_1 = 0.0258$ and 0.0464, respectively. This compares to $R_1 = 0.0500$ and 0.0515 for the wrong model, i.e., the one with the positions left unswitched (Yb analog model). In addition, when these two sites are positioned as in the Yb analog, the thermal displacement parameters become unreasonable. Data collection and structure refinement details are given in Table 1. The final atomic positions and equivalent isotropic displacement parameters are given in Table 2, and selected bond distances are listed in Table 3.

To determine phase identity and purity, we collected powder X-ray diffractions patterns of the $RE_7Co_4InGe_{12}$ at room temperature on a CPS 120 INEL diffractometer with Cu Ka radiation and equipped with a position-sensitive detector.

Differential Thermal Analysis. Differential thermal analysis (DGA) was conducted with a Shimadzu TDA-50 analyzer. The sample was flame-sealed under a reduced atmosphere in fused silica ampoules that were carbon-coated to prevent glass attack upon melting of the products. α-Al_2O_3 standard was used as a reference. The analysis was performed by heating the sample to 1000 °C at a rate of 10 °C per min, holding it at 1000 °C for 1 min, cooling it to 100 °C at the same rate, and then repeating the cycle.

(19) Sheldrick, G. M. *SADABS* and *SAINT*, version 4; University of Göttingen: Göttingen, Germany, 1995.
(20) Sheldrick, G. M. *SHELXTL, Structure Determination Program*, version 5.0; Siemens Analytical X-ray Instruments, Inc.: Madison, WI, 1995.
(21) Farrugia, L. J. *WinGX, Solution, Refinement and Analysis of Single Crystal X-Ray Diffraction Data*, version 1.70.01; University of Glasgow: Glasgow, Scotland, 1997−2005.

Table 1. Crystallographic Data for $RE_7Co_4InGe_{12}$ (RE = Dy, Ho, Yb)

	$Dy_7Co_4InGe_{12}$	$Ho_7Co_4InGe_{12}$	$Yb_7Co_4InGe_{12}$
fw	2359.12	2376.13	2432.90
cryst syst	tetragonal	tetragonal	tetragonal
space group	*P*4/*m*	*P*4/*m*	*P*4/*m*
a (Å)	10.3522(5)	10.357(3)	10.2937(7)
b (Å)	10.3522(5)	10.357(3)	10.2937(7)
c (Å)	4.1784(5)	4.1538(15)	4.1518(5)
V (Å^3)/*Z*	447.79(6)/1	445.6(2)/1	439.93(7)/1
D_{calcd} (mg/m^3)	8.748	8.855	9.183
absorp coeff (mm^{-1})	53.380	55.370	61.813
index ranges	$-13 \le h \le 13$, $-13 \le k \le 13$, $-5 \le l \le 5$	$-13 \le h \le 13$, $-13 \le k \le 13$, $-5 \le l \le 5$	$-12 \le h \le 13$, $-13 \le k \le 12$, $-5 \le l \le 5$
no. of reflns collected/unique/$R_{(int)}$	4986/607/ 0.0498	4844/606/ 0.0364	4942/612/ 0.0461
data/restraints/params	607/0/40	606/0/40	612/0/40
GOF on F^2	1.138	1.299	1.126
final *R* indices [$I > 2\sigma(I)$] (R_1/wR_2)[a]	0.0258/0.0552	0.0464/0.1141	0.0304/0.0710
R indices (all data) (R_1/wR_2)[a]	0.0336/0.0580	0.0496/0.1152	0.0332/0.0723
extinction coeff	0.0069(4)	0.0042(5)	0.0090(5)
largest diff. peak and hole (e Å^{-3})	1.444 and −2.178	6.830 and −3.493	3.620 and −1.670

[a] $R_1 = \sum||F_o| - |F_c||/\sum|F_o|$; $wR_2 = [\sum w\{|F_o| - |F_c|\}^2/\sum w|F_o|^2]^{1/2}$; $w = 1/\sigma^2\{|F_o|\}$.

Table 2. Atomic Coordinates ($\times 10^4$) and Equivalent Isotropic Displacement Parameters (Å$^2 \times 10^3$) for $RE_7Co_4InGe_{12}$ (RE = Dy, Ho, Yb)

atom	Wyckoff	x	y	z	U_{eq}[a]
Dy(1)	4*k*	3232(1)	3259(1)	5000	7(1)
Dy(2)	1*a*	0	0	0	8(1)
Dy(3)	2*f*	0	5000	5000	8(1)
Ge(1)	4*j*	2139(1)	5124(1)	0	7(1)
Ge(2)	4*j*	1131(1)	2860(1)	0	10(1)
Ge(3)	4*k*	1950(1)	655(1)	5000	11(1)
Co	4*j*	2797(1)	1181(1)	0	7(1)
In	1*c*	5000	5000	0	8(1)
Ho(1)	4*k*	3245(1)	3260(1)	5000	8(1)
Ho(2)	1*a*	0	0	0	8(1)
Ho(3)	2*f*	0	5000	5000	10(1)
Ge(1)	4*j*	2139(2)	5102(2)	0	10(1)
Ge(2)	4*k*	1133(3)	2853(3)	0	18(1)
Ge(3)	4*j*	−664(3)	1957(3)	5000	17(1)
Co	4*j*	2811(3)	1182(3)	0	9(1)
In	1*c*	5000	5000	0	9(1)
Yb(1)	4*k*	3262(1)	3243(1)	5000	5(1)
Yb(2)	1*a*	0	0	0	5(1)
Yb(3)	2*f*	0	5000	5000	7(1)
Ge(1)	4*j*	2164(1)	4886(1)	0	5(1)
Ge(2)	4*j*	2865(2)	1130(1)	0	12(1)
Ge(3)	4*k*	679(2)	1931(1)	5000	9(1)
Co	4*j*	1191(2)	2800(2)	0	5(1)
In	1*c*	5000	5000	0	7(1)

[a] U_{eq} is defined as one-third of the trace of the orthogonalized U_{ij} tensor.

Table 3. Selected Bond Lengths (Å) for $RE_7Co_4InGe_{12}$

bond	RE = Dy	RE = Ho	RE = Yb
RE(1)−Ge(1)	2.9336(9)	2.932(1)	2.9060(10)
RE(1)−Ge(3)	3.0048(13)	3.001(3)	2.9820(16)
RE(1)−Co	3.0329(11)	3.025(2)	3.0102(13)
RE(1)−Ge(1)	3.0610(9)	3.043(2)	3.0298(10)
RE(1)−Ge(2)	3.0441(9)	3.045(2)	3.0340(11)
RE(1)−In	3.3109(4)	3.2965(11)	3.2838(5)
RE(1)−RE(1)	3.6324(8)	3.6204(18)	3.5983(8)
RE(2)−Ge(3)	2.9829(9)	2.983(2)	2.9575(10)
RE(2)−Co	3.1428(14)	3.158(3)	3.1323(17)
RE(3)-Ge(1)	3.0473(9)	3.039(2)	3.0473(10)
RE(3)−Ge(3)	3. 2300(12)	3. 226(3)	3.2360(15)
RE(3)−Ge(2)	3.2620(9)	3.262(2)	3.2392(12)
RE(3)−Co	3.3257(11)	3.309(3)	3.3074(14)
Ge(1)−Co	2.3702(18)	2.378(4)	2.369(2)
Ge(1)−Ge(2)	2.5652(17)	2.552(4)	2.548(2)
Ge(1)−In	2.9643(12)	2.965(3)	2.9214(14)
Ge(2)−Co	2.3937(19)	2.398(4)	2.390(2)
Ge(2)−Co	2.4493(19)	2.453(4)	2.434(2)
Ge(3)−Co	2.3302(9)	2.3203(19)	2.3213(10)

Magnetic Measurements, Magnetic susceptibility measurements were carried out with a Quantum Design MPMS SQUID magnetometer. EDS-analyzed crystals were soaked in ~ 6 M HCl acid for 15−30 min, washed with water, and dried in a dry oven. The crystals were then randomly placed and sealed in Kapton tape, which was inserted into the SQUID magnetometer. Temperature-dependent data were collected between 3 and 400 K, with an applied field of 500 G. Field-dependent magnetic measurements were acquired at 3 K with field sweeping from −50000 to 50000 G.

X-ray Photoemission Spectroscopy. X-ray photoemission spectroscopy was performed on a Perkin-Elmer Phi 5400 ESCA system equipped with a Magnesium Kα X-ray source. Samples were analyzed at pressures between 1×10^{-9} and 1×10^{-8} Torr with a pass energy of 29.35 eV and a takeoff angle of 45°. The spot size was roughly 250 μm^2. All peaks were referenced to the signature C1s peak for adventitious carbon at 284.6 eV.

X-ray Absorption Near-Edge Spectroscopy (XANES). X-ray absorption fine structure (XAFS) experiments were performed in Sector 20, bending magnet beamline (PNC/XOR, 20-BM), of the Advanced Photon Source at the Argonne National Laboratory, IL. Measurements at the Yb L_{III} edge were performed in the transmission mode using gas ionization chambers to monitor the incident and transmitted X-ray intensities. A third ionization chamber was used in conjunction with a copper foil to provide internal calibration for the alignment of the edge positions. Monochromatic X-rays was obtained using a Si (111) double crystal monochromator. The monochromator was calibrated by defining the inflection point (first derivative maxima) of Cu foil as 8980.5 eV. A Rh-coated X-ray mirror was utilized to suppress higher-order harmonics. XAFS samples were prepared by mixing an appropriate amount of the finely ground Yb compound with BN. The mixture was pressed to form a self-supporting pellet, which was mounted on the cold finger of a closed-cycle refrigerator. Measurements were performed at a range of temperatures from 15 to 300 K using a closed cycle refrigerator. Care was taken to suppress distortion in the data from thickness effects.

Magnetotransport Measurements. Magnetotransport measurements were performed on a needle-shaped sample with approximate dimensions of 648 × 56 × 75 μm^3 and with the long direction oriented parallel to the crystallographic *c*-axis. Four gold wires were attached with silver paint, and the resistance of the sample was obtained in a standard four-probe measurement with a current of 100 μA. By averaging the sample voltage corresponding to positive and negative currents, we eliminated artifacts due to the thermal

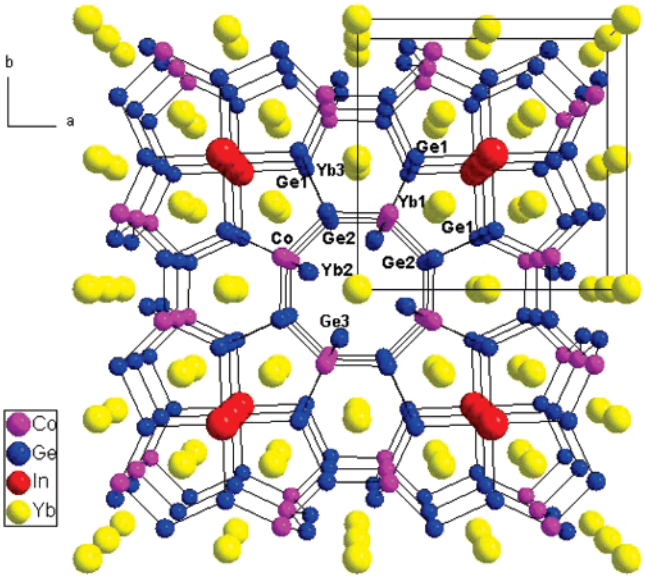

Figure 2. Overall structure of $Yb_7Co_4InGe_{12}$ as viewed onto the *a*,*b*-plane. For clarity, the bonds to the Yb atoms are not drawn.

voltages. The sample was inserted into a superconducting magnet equipped with a variable-temperature insert that allows controlling of the sample's temperature between 1.2 and 320 K. The magnetic field was oriented perpendicular to the needle.

Results and Discussion

Reaction Chemistry. $Yb_7Co_4InGe_{12}$ was first observed from indium flux as silvery thin needles frequently aggregated in bundles. Figure 1 shows a scanning electron micrograph of a typical $Yb_7Co_4InGe_{12}$ crystal. Other reaction products included Yb_2InGe_2,[22,23] $Yb_5Co_4Ge_{10}$,[24] the cubic phase $YbIn_3$ and recrystallized germanium. Subsequent tuning of the reaction conditions increased the yield and eliminated all byproducts except Yb_2InGe_2, which was easily distinguishable, because of its very different crystal morphology. When other RE metals such as La, Ce, Sm, Eu, Dy, Ho, and Er were employed under the same reaction conditions, only Dy and Ho were able to form the same phase but in much smaller yield. This suggests that the size of the rare-earth cations likely plays a decisive role for the formation of $RE_7Co_4InGe_{12}$. The $Yb_7Co_4InGe_{12}$ compound does not melt up to 1000 °C, as confirmed by differential thermal analysis.

Structure. The $RE_7Co_4InGe_{12}$ (RE = Dy, Ho, Yb) compounds crystallize in the tetragonal *P*4/*m* space group in what appears to be a new structure type. Because of their isostructural nature, we will describe the structure in terms of the $Yb_7Co_4InGe_{12}$ analog. The overall structure of $Yb_7Co_4InGe_{12}$ as viewed down the *c*-axis is depicted in Figure 2. The bonds to the Yb atoms were omitted to emphasize the three-dimensional (3D) $[Co_4InGe_{12}]$ framework and its channels. This network is characterized by three different

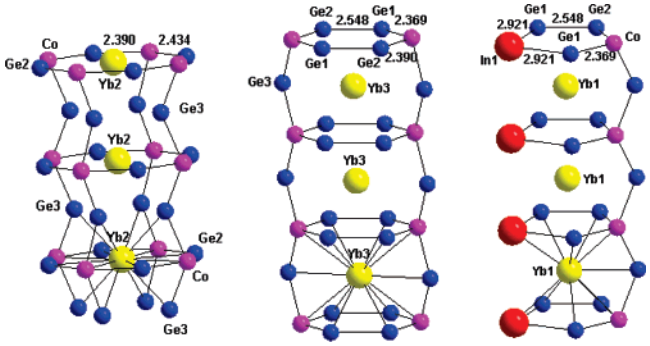

Figure 3. The octagonal, hexagonal, and pentagonal rings and their interconnection to form the corresponding tunnels running down the *c*-axis. The coordination environment of the Yb atoms is also highlighted. The coordination sphere cutoff is 3.4 Å.

types of channels, propagating along the *c*-axis, in which the Yb atoms are situated. Another way to look at the $[Co_4InGe_{12}]$ substructure is in terms of columns of octagonal and hexagonal rings that run along the axis, whereas the void space between them is filled up by four pentagons related by the 4-fold axis of the tetragonal symmetry. The polygonal rings are connected down the *c*-axis via Co−Ge(3) Co zigzag chains.

The biggest channels in the structure are built from stacked alternating planar layers of distorted octagons and square planes, Figure 3. The octagons are comprised from alternating Co and Ge(2) atoms, whereas the Yb(2) atoms are sitting in their center. The two Co−Ge(2) interatomic distances at 2.390(2) and 2.434(2) Å fall in the Co−Ge bond range found in other binary or ternary intermetallics.[25,26] Similar octagonal channels can be found in Yb_5TMGe_{10}[24] and in general in the $RE_5TM_4X_{10}$ series[27,28] (RE = rare earth, Sc, or Y; TM = Co, Rh, Ir, or Os; and X = Si, Ge, or Sn), where they all adopt the tetragonal $Sc_5Co_4Si_{10}$ (*P*4/*mbm*) structure.[29]

Another structural feature is the hexagonal tunnels, Figure 3. In these, two Ge(1)−Ge(2) dimers are interconnected with two Co atoms to form distorted hexagonal rings that are stacked parallel to the *c*-axis and are connected via Ge(3) atoms. In contrast to the octagonal tunnels, here, the Yb(3) atoms are sandwiched between the hexagons. The Ge(1)−Ge(2) interatomic distances at 2.548(2) Å are comparable with Ge−Ge contacts observed in many RE germanides with 2D and 3D networks, including $Ho_5Rh_4Ge_{10}$[27] at 2.539 Å.

The final noteworthy structural moiety is the pentagonal channels, which are fused in groups of four that share a central column of square planar In atoms, see Figure 2. A Ge(1)−Ge(2) dimer is linked to a Co and an In atom from the Ge(2) and Ge(1) site, correspondingly; both of them connect to another Ge(1) atom, thus forming pentagonal rings that extend along the *c*-axis through one Co−Ge(3)−Co

(22) Zaremba, V. I.; Tyvanchuk, Y. B.; Stepien-Damm, J. *Z. Kristallogr.−New Cryst. Struct.* **1997**, *212* (2), 291−291.
(23) Tobash, P. H.; Lins, D.; Bobev, S.; Lima, A.; Hundley, M. F.; Thompson, J. D.; Sarrao, J. L. *Chem. Mater.* **2005**, *17* (22), 5567−5573.
(24) Katoh, K.; Tsutsumi, T.; Yamada, K.; Terui, G.; Niide, Y.; Ochiai, A. *Physica B* **2006**, *373* (1), 111−119.
(25) Mruz, O. Y.; Belsky, V. K.; Gorelenko, Y. K.; Skolozdra, R. V.; Bodak, O. I. *Ukr. Fiz. Zh.* **1987**, *32* (12), 1856−1858.
(26) Welter, R.; Venturini, G.; Malaman, B.; Ressouche, E. *J. Alloys Compd.* **1993**, *201*, 191−196.
(27) Patil, N. G.; Ramakrishnan, S. *Phys. Rev. B* **1999**, *59* (14), 9581−9589.
(28) Becker, B.; Patil, N. G.; Ramakrishnan, S.; Menovsky, A. A.; Nieuwenhuys, G. J.; Mydosh, J. A. *Phys. Rev. B* **1999**, *59* (11), 7266−7269.
(29) Braun, H. F.; Yvon, K.; Braun, R. M. *Acta Crystallogr., Sect. B* **1980**, *36*, 2397−2399.

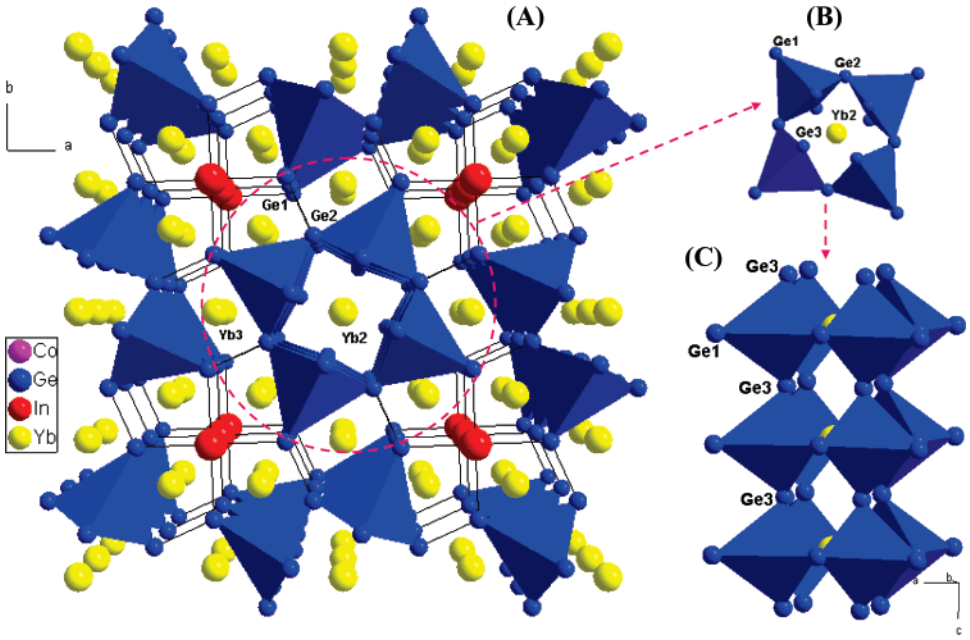

Figure 4. (A) Polyhedral view of the $Yb_7Co_4InGe_{12}$ structure featuring the connectivity between Co-centered Ge tetragonal pyramids. (B) The polyhedra share Ge(2) corners to form squares. (C) Stacking of squares along the *c*-axis forming square tubes.

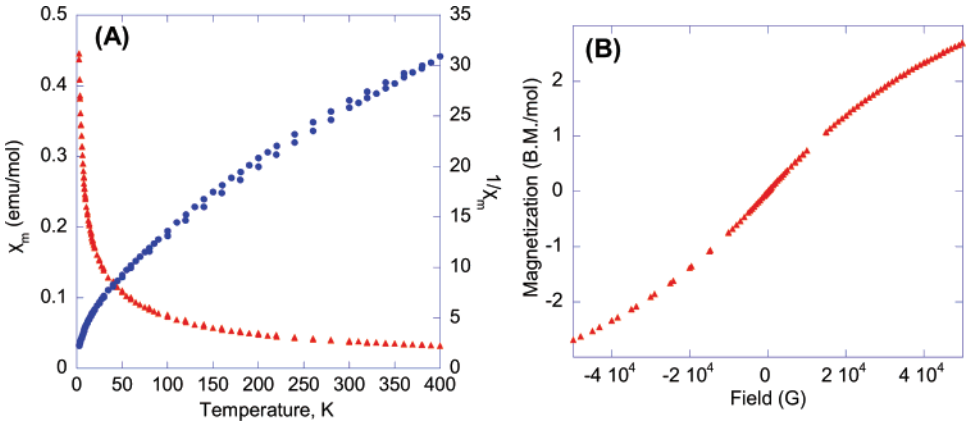

Figure 5. Temperature dependence of the molar susceptibility χ_m (triangles) and inverse $1/\chi_m$ (circles) for $Yb_7Co_4InGe_{12}$ with an applied field of 500 G. (B) Magnetization data for $Yb_7Co_4InGe_{12}$ collected at 3 K.

zigzag chain (Figure 3). The Co−Ge(2) and Co−Ge(1) distances at 2.434(2) and 2.369(2) Å, respectively, are found in the two other types of rings. The four-coordinated In atoms are bonded to four Ge(1) atoms (with In−Ge(1) bond at 2.9214(14) Å) in a square-planar environment. This is a rare coordination environment for a group 13 element. A similar In coordination environment was also found in RE_2InGe_2.[22,23] In the pentagonal channels, as in the case of the hexagonal ones, the Yb(1) atoms are located between the pentagonal layers. There are no direct Co−Co bonds in the structure.

An alternative way to view the $Yb_7Co_4InGe_{12}$ structure is in polyhedral representation. Figure 4A depicts the connectivity of the Co-centered Ge tetragonal pyramids as viewed down the *c*-axis. Four such polyhedra share their Ge(2) corners in the *a*,*b*-plane, forming square rings, see Figure 4B. These squares stack along the *c*-axis by connecting trough the Ge(3) corners of the pyramids to form square tubes that extend down the *c*-axis, Figure 4C. These tubes are aligned parallel to each other, and every such tube is connected directly to four other neighboring tubes through Ge(1)−Ge(2) bonds at 2.548(2) Å to build the 3D [Co_4InGe_{12}] framework. The Yb(2) atoms reside within the tubes, whereas Yb(1) and Yb(3) atoms are located between adjacent square tunnels.

The local coordination environments (within 3.5 Å) of the RE atoms are illustrated in Figure 3. RE(1) atoms are 11-coordinate and sitting in the center of a pentagonal prism, made up of six Ge(1), two Co, and two In atoms, and capped with one Ge(3) atom. The RE(2) atoms have 16 neighbors in their immediate coordination sphere. These include four Ge(2) and four Co atoms in a form of a flat octagonal ring (where the RE(2) is the center) and eight additional Ge(3) atoms with four located above and four below the octagon in a square prismatic geometry. Finally, RE(3) exhibit a coordination number of fourteen, in an arrangement that is best described as a hexagonal prism comprising four Ge(1), four Ge(2), and four Co atoms, capped by two Ge(3) atoms.

Magnetic Measurements. Magnetic susceptibility data for $Yb_7Co_4InGe_{12}$are presented in Figure 5A. The temperature dependence of the molar susceptibility (χ_m) displays paramagnetic behavior suggesting the existence of Yb^{3+} moments in the material. No magnetic ordering was observed down

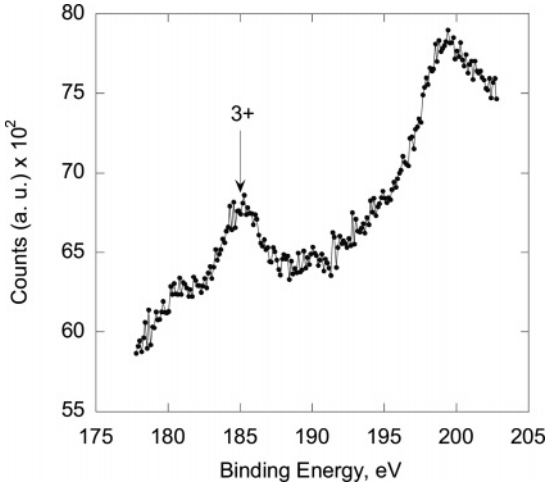

Figure 6. XPS spectra of Yb 4d core level for $Yb_7Co_4InGe_{12}$ at 300 K.

to 3.5 K. The inverse susceptibility does not follow the Curie−Weiss law especially at the temperature region below 100 K, which can be attributed to crystal-field contributions and/or to a possible onset of a valence fluctuation. The weak linearity of the data precluded the unequivocal determination of the μ_{eff}. However, analyzing the susceptibility data in a proper temperature range ($T > 100$ K) with the modified Curie−Weiss law $\chi(T) = \chi_0 + C/(T - \theta_p)$ yields information concerning the sum of the temperature-independent contributions χ_o, e.g., van Vleck paramagnetism, paramagnetism due to conduction electrons, and core−electron diamagnetism, the effective magnetic moment μ_{eff} (deduced from the Curie constant C), and the Weiss constant θ_p. A nonlinear least-squares fit to this equation resulted in $\chi_0 = 1.9 \times 10^{-3}$ emu/mol Yb, $\theta_p = -38$ K, indicating antiferromagnetic interactions among the Yb atoms, and an effective moment of 3.1 μ_B/Yb, which is ~68% of the value expected for the free-ion Yb^{3+}, 4.54 μ_B. This means that more than half of the Yb atoms are in the Yb^{3+} state. This is supported by the XANES studies presented below.

The field-dependence of magnetization for $Yb_7Co_4InGe_{12}$ at 3 K can be found in Figure 5B. The magnetization increases linearly up to a field of 20 kG, at which point the slope continuously changes until approximately 33 kG, where it becomes linear again, but with a much shallower slope. The response remains linear up to the highest attainable field, with no signs of saturation up to 50 kG. The moment reaches a value of only 2.7 μ_B, which is about 67.5% of the value anticipated for the fully saturated moment of an Yb^{3+} ion.

XPS Measurements. To further probe the Yb oxidation state in $Yb_7Co_4InGe_{12}$, we performed X-ray photoelectron spectroscopy (XPS) measurements. The XPS spectrum revealed a strong peak at ~185 eV and a multiplet structure at higher energies (Figure 6). This type of spectrum, is consistent with the presence of Yb^{3+} ions.[30,31] With careful inspection of the spectra, we see two very weak peaks at ~181 and 191 eV. This double peak is known from the literature that is attributed to Yb^{2+} ions.[30]

XANES Measurements. Because XPS is a surface analytical technique, it was crucial to carry out X-ray absorption near-edge spectroscopy (XANES) measurements at the Yb L_{III} edge, which is an established method for studying the valence of the absorbing element. XANES fundamentally probes the bulk of the sample. The near-edge spectra of a $Yb_4Co_7InGe_{12}$ sample obtained at 15 and 300 K are given in Figure 7A. The main absorption peak (white line) for both spectra is centered at ~8948 eV, which is typical of trivalent Yb, both in oxide form as well as in Yb intermetallics.[32−34] Relative to Yb^{3+}, divalent Yb exhibits a white line that is ~8 eV lower in energy.[32−34] The spectra also reveal the presence of a weaker feature (shoulder) at ~8940 eV, indicating that some divalent Yb is also present.

Another interesting observation in the XANES spectra is that the relative ratio of the features at 8940 and 8948 eV varies weakly with temperature. In particular, with increasing temperature, the low-energy peak originating from Yb^{2+} ion is slightly depressed, whereas the high-energy one originating from Yb^{3+} ion is enhanced, suggesting that the average valence of Yb is slightly temperature dependent and that the Yb^{3+} state is more populated at higher temperatures. Similar behavior was observed in the $YbCu_{5-x}Ga_x$ series.[35] Figure 7B displays both the spectra of the present phase and Yb_2O_3 at room temperature. To ensure that we are not observing spectra from oxide impurities, we also computed and compared the XAFS of $Yb_4Co_7InGe_{12}$ with that of Yb_2O_3 standard. The absence of Yb−O bonds shows that the Yb in the sample is not coordinated to oxygen, indicating that the trivalent character is intrinsic to $Yb_4Co_7InGe_{12}$.

An attempt to obtain the relative amount of Yb^{3+} and Yb^{2+} was performed by representing the normalized Yb XANES as a pair of pseudo-Voigt and modified arc-tangent functions. We estimate the amount of Yb^{3+} to be ~73% with an error of ~15%. A more accurate determination of Yb valence will require measurements of Yb^{2+} and Yb^{3+} standards (or analogs) with similar structure to the sample under study and will be a subject of future investigations.

Magnetotransport Measurements. The temperature dependence of the resistivity (ρ) for samples of $Yb_4Co_7InGe_{12}$ with and without the application of magnetic field is shown in Figure 8. The resistivity data measured on single crystals along the c-axis and at zero applied field reveal a rather moderate metallic behavior with $\rho \approx 205$ $\mu\Omega$ cm at 246 K. The inset in Figure 8 displays the low-temperature ρ data at a field of 0, 1, and 5 T applied perpendicular to the c-axis. It can be clearly seen that the material displays negative magnetoresistance at low temperatures (i.e., the resistivity drops with increasing applied field). This behavior is

(30) Chung, J. S.; Cho, E. J.; Oh, S. J. *Phys. Rev. B* **1990**, *41* (9), 5524−5528.
(31) Szytula, A.; Jezierski, A.; Penc, B.; Winiarski, A.; Leithe-Jasper, A.; Kaczorowski, D. *J. Alloys Compd.* **2003**, *360* (1−2), 41−46.
(32) Rao, C. N. R.; Sarma, D. D.; Sarode, P. R.; Sampathkumaran, E. V.; Gupta, L. C.; Vijayaraghavan, R. *Chem. Phys. Lett.* **1980**, *76* (3), 413−415.
(33) Hatwar, T. K.; Nayak, R. M.; Padalia, B. D.; Ghatikar, M. N.; Sampathkumaran, E. V.; Gupta, L. C.; Vijayaraghavan, R. *Solid State Commun.* **1980**, *34* (8), 617−620.
(34) Moreschini, L.; Dallera, C.; Joyce, J. J.; Sarrao, J. L.; Bauer, E. D.; Fritsch, V.; Bobev, S.; Carpene, E.; Huotari, S.; Vanko, G.; Monaco, G.; Lacovig, P.; Panaccione, G.; Fondacaro, A.; Paolicelli, G.; Torelli, P.; Grioni, M. *Phys. Rev. B* **2007**, *75* (3).
(35) Bauer, E.; Tuan, L.; Hauser, R.; Gratz, E.; Holubar, T.; Hilscher, G.; Michor, H.; Perthold, W.; Godart, C.; Alleno, E.; Hiebl, K. *Phys. Rev. B* **1995**, *52* (6), 4327−4335.

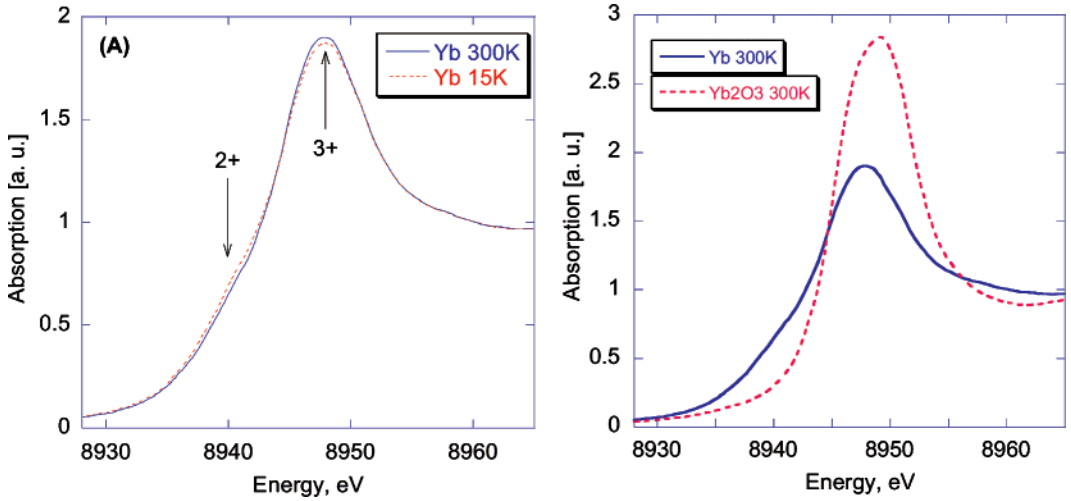

Figure 7. (A) L_{III} absorption edge spectra of Yb in $Yb_7Co_4InGe_{12}$ at 15 K (dashed line) and 300 K (solid line). (B) Comparison of $Yb_7Co_4InGe_{12}$ and Yb_2O_3 spectra at room temperature.

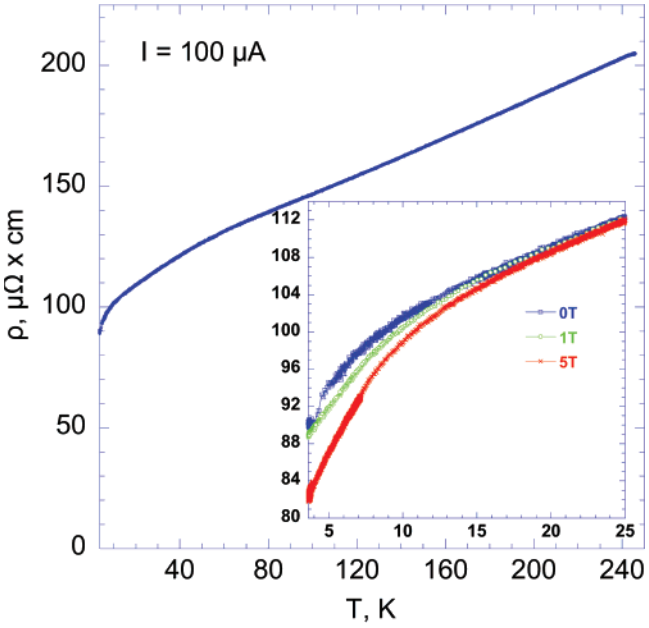

Figure 8. Variable-temperature single-crystal resistivity data for $Yb_7Co_4InGe_{12}$ at zero field. Inset: low-temperature resistivity data at 0, 1, and 5 T field.

frequently seen in many Kondo or heavy fermion systems and is attributed to the suppression of scattering of the conduction electrons from the unpaired f-electrons in a high field.

Both magnetic susceptibility and XANES measurements suggest that the $Yb_4Co_7InGe_{12}$ is a new heterogeneous mixed-valence compound, i.e., a system with both Yb^{3+} and Yb^{2+} sites with about two thirds of the Yb atoms being in the Yb^{3+} (f^{13}) state. Because there are three crystallographically distinct Yb sites, we can possibly speculate that two of them have atoms in the Yb^{3+} configuration and one in the Yb^{2+} configuration. To assign which site could possibly accommodate Yb^{2+} ions, we can compare the coordination environment of each Yb site. The nearest-neighbor distances for Yb(1) are 2.9060 (Yb−Ge) and 3.0102 (Yb−Co) Å, respectively, whereas those for the Yb(2) site are 2.9575 (Yb−Ge) and 3.1323 (Yb−Co) Å, respectively. The corresponding distances for the Yb(3) site are 3.0473 (Yb−Ge) and 3.3074 (Yb−Co) Å, respectively. Because the distances around the Yb(3) sites are considerably longer than those of the other two sites, a plausible conclusion is that the Yb^{2+} ions with their larger ionic radius probably occupy the Yb(3) site.

In conclusion, three new quaternary $RE_7Co_4InGe_{12}$ phases crystallize in molten In under a new structure type. The flux seems necessary to stabilize these compounds because direct combination of the elements and induction heating reactions with various stoichiometric ratios failed so far to form them. In general, when studying systems of the type RE/TM/Ge in liquid In, the tendency is for In not to get incorporated into the compound. In the case of $RE_7Co_4InGe_{12}$, we observe the reactive nature of the flux, where In enters the structure and produces a new structure type. The $Yb_7Co_4InGe_{12}$ is a mixed-valence compound with a high Yb^{3+}/Yb^{2+} ratio that is slightly temperature dependent. Because of the small yields of the other two analogs, complete property characterization could not be performed. Nevertheless, preliminary magnetic susceptibility measurements for $Dy_7Co_4InGe_{12}$ indicate ferromagnetic ordering below 30 K.

Acknowledgment. This work was supported by UChicago Argonne, LLC, Operator of Argonne National Laboratory. Argonne, a U.S. Department of Energy Office of Science Laboratory, is operated under Contract DE-AC02-06CH11357. PNC/XOR facilities and research at these facilities are supported by the U.S. DOE and its founding institutions. We thank the Department of Energy for Grant DE-FG02-07ER46356.

Supporting Information Available: Ansisotropic displacement parameters table, preliminary magnetic measurement data for $Dy_7Co_4InGe_{12}$, and XAFS data for $Yb_7Co_4InGe_{12}$ (PDF); crystallographic information in CIF format. This material is available free of charge via the Internet at http://pubs.acs.org.

CM071687Q